JACS
JOURNAL OF THE AMERICAN CHEMICAL SOCIETY
Article
pubs.acs.org/JACS

Controllable Drug Release and Simultaneously Carrier Decomposition of SiO_2-Drug Composite Nanoparticles

Silu Zhang,[†] Zhiqin Chu,[†] Chun Yin,[‡] Chunyuan Zhang,[‡] Ge Lin,*[,‡] and Quan Li*[,†]

[†]Department of Physics and [‡]School of Biomedical Sciences, Faculty of Medicine, The Chinese University of Hong Kong, Shatin, New Territories, Hong Kong

Supporting Information

ABSTRACT: Drug release simultaneously with carrier decomposition has been demonstrated in SiO_2-drug composite nanoparticles. By creating a radial drug concentration gradient in the nanoparticle, controllable release of the drug is primarily driven by diffusion. Escape of the drug molecules then triggers the SiO_2 carrier decomposition, which starts from the center of the nanoparticle and eventually leads to its complete fragmentation. The small size of the final carrier fragments enables their easy excretion via renal systems. Together with the known biocompatibility of SiO_2, the feature of controllable drug release and simultaneous carrier decomposition achieved in the SiO_2-drug nanoparticles make it ideal for a wide range of diagnostic and therapeutic applications with great promise for potential clinical translation.

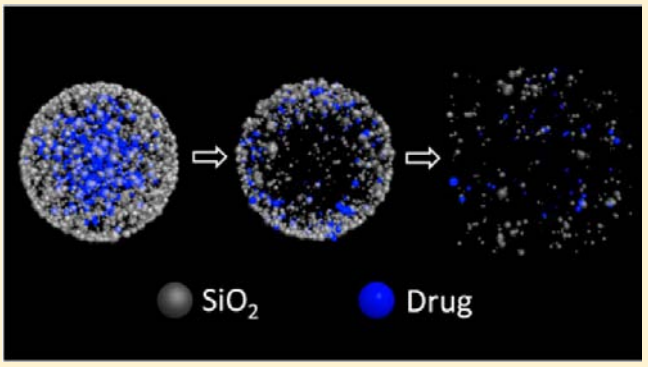

INTRODUCTION

An ideal nanoparticle (NP) carrier-drug system has several features, including effective cellular uptake, controllable release, and safe excretion from the biological system after functioning. Improved cellular uptake has been claimed in several NP carrier-drug systems,[1−6] in which the drug molecules can be disguised by residing inside the carrier, while the carrier surface is hydrophilic for easy cellular uptake. Controllable release (with a desired releasing rate and duration) of the drug molecules from the carrier guarantees relatively stable therapeutic levels during the treatment period.[7] Nevertheless, this task remains challenging in most of the NP carrier-drug systems. Elimination of the drug/drug carriers from the biologic system after their carrying out the diagnostic or therapeutic functions is another important aspect to consider. Unfortunately, this remains as one of the major obstacles impeding potential clinical translation of NP carrier-drugs. It has been found that the hydrodynamic size required for renal clearance is too small (<5.5 nm)[8] to enable the incorporation of adequate amounts of multifunctional components (e.g., for targeting, therapy, etc.), and rapid renal excretion reduces the time available to the NPs to carry out its function. On the other hand, although materials of larger sizes (e.g., ∼20−200 nm) may provide host spacious enough for functionality loading and have prolonged residence time in the bloodstream, they avoid renal filtration, leading to increased toxicity at system level.[9,10] A most desirable design for improving the biocompatibility of NP carrier-drug would involve the incorporation of controllable drug release together with carrier self-destruction, through which the carrier could be hierarchically degraded into harmless, renally clearable products[11,12] after the drug carrying out their function.

Silica NPs are considered as one of the most promising carrier systems, as it is generally accepted as nontoxic,[13,14] and provide a versatile platform for drug loading.[15] The surface of the SiO_2 NP is hydrophilic, being favorable for cellular uptake. Three generic strategies have been developed for drug loading into the SiO_2 NP carrier, i.e., with the drug molecules being embedded in the dense SiO_2 NPs, residing in the pores of mesoporous SiO_2 NPs (MSN) and being attached on the surface of the NPs, via chemical bonding or physical adsorption.[4,16−19] Moderate success in drug release has been achieved in some systems, when the gradual release of drug is controlled by morphological characteristics of the NP carriers. For example, release of drugs has been reported via diffusion using MSN with various pore morphologies.[20] Alternatively drug release triggered by diverse physical and chemical stimuli has been realized via gated mechanisms on mesoporous scaffolds. In the gated MSN, the pores loaded with guest molecules are capped by NPs via a cleavable linkage, by deformable polymers, or by chemical molecules/biomolecules. The guest molecules can then be released by removing the caps via external stimuli, such as photon, thermal, or pH changes, etc.[21−25] Nevertheless, none of these configurations can simultaneously satisfy the above three criteria, in particular, the controlled release and carrier self-destruction to very small sized fragments are highly desired but not realized.

Received: December 17, 2012
Published: March 18, 2013

   dx.doi.org/10.1021/ja3123015 | J. Am. Chem. Soc. 2013, 135, 5709−5716

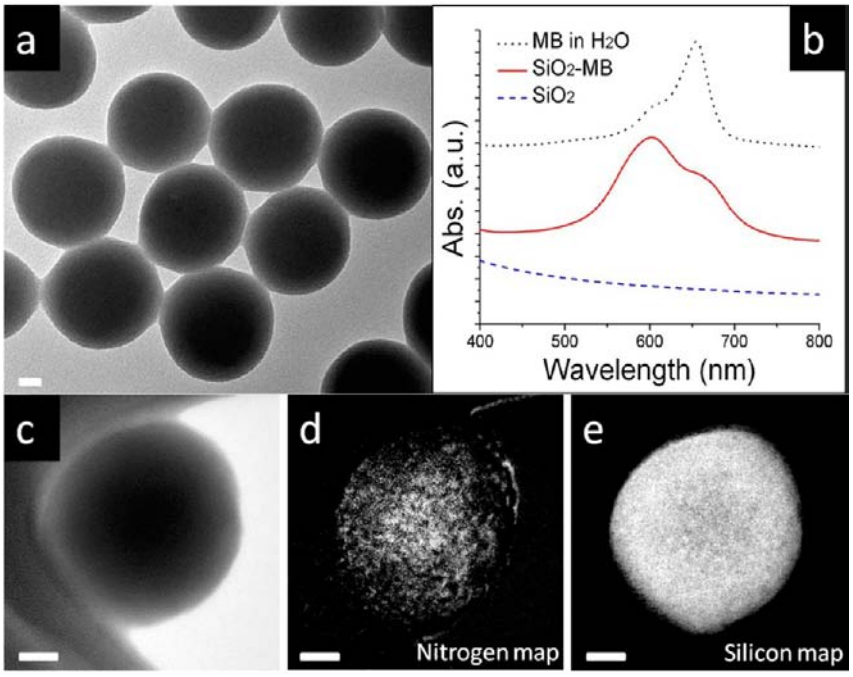

Figure 1. Characterizations of SiO_2-MB NPs. (a) Typical TEM image of the SiO_2-MB NPs. (b) Absorption spectra taken from pure MB, SiO_2-MB NPs, and pure SiO_2 NPs in aqueous solutions. (c) Filtered bright-field TEM image of single NP and the corresponding EELS maps of (d) nitrogen and (e) silicon. The scale bar is 20 nm.

In the present work, we have developed a special type of SiO_2-drug composite NPs by introducing drug molecules into SiO_2 during the NP growth at controlled experimental conditions. Taking methylene blue (MB) as an example, we show that by creating a radial concentration gradient of MB in the NP, MB release occurs simultaneously with the SiO_2 carrier decomposition, as driven by drug molecule diffusion. The key factors that determine the specific MB release and SiO_2 carrier decomposition characteristics are identified. The experimental results suggest a most attractive and promising NPs carrier-drug system for diagnostic and therapeutic applications. We also shown that such simple growth mechanism can be applied to many other molecules employing the SiO_2 NP carrier, with the same feature achieved.

RESULTS AND DISCUSSION

Characterization of SiO_2-MB NPs. Figure 1a showed a typical transmission electron microscopy (TEM) image of the as-synthesized silica-MB NPs. They were spherical in shape with an average diameter of ~80 nm. Successful incorporation of the MB into the NPs was suggested by the absorption spectrum taken from the NP sample. Compared to the pure MB absorption measured in aqueous solution, its characteristic absorption at ~665 nm (for monomer absorption) and ~600 nm (for dimer absorption) were clearly observed in the SiO_2-MB NP sample but not in the control sample containing pure SiO_2 NPs (Figure 1b). The relatively higher intensity of the dimer absorption peak (as compared to the monomer one) indicated aggregation of MB molecules, which occurred when they were grown into the SiO_2 NPs.[16] This served as an additional piece of evidence that MB resided inside the SiO_2 NPs.

Further evidence of MB incorporation and information on their spatial distribution inside the NP was provided by chemical maps obtained using electron energy loss spectroscopy (EELS). Figure 1c–e gave the filtered bright-field TEM image of one such NP and the corresponding chemical maps taken from two compositional elements: Si and N (a major compositional element of MB). Nonuniform distribution of both Si and N was observed, i.e., N was found to be more concentrated in the center of the NP, whereas Si was deficient. By removing the thickness contribution in the elemental mapping, the abundance profile of N was obtained, in which one can see a decreasing N amount from the center to the surface of the NPs (Figure S1a). Further evidence on the feature of "central concentrated MB" was obtained by calcination of the NPs at elevated temperatures, when the MB molecules were removed and center-hollow SiO_2 NPs were obtained (Figure S1b).

Controllable Drug Release and Simultaneously Carrier Decomposition of SiO_2-MB NPs. Absorption spectra were taken from both the NPs (dried and then redispersed in water) (Figure 2a) and the supernatant (Figure 2b) of sample M1 (with MB loading amount as 75 μg MB/mg NP), after the NPs had been immersed in deionized water for specified period of times (2 h and 1–3, 6, 9, and 14 days) at room temperature. The released chemical in the supernatant has two characteristic absorptions at ~665 and ~600 nm, which agree with the monomer and dimer absorption of MB, respectively. This result suggests the chemical integrity of MB when being encapsulated into the silica NPs (Further evidence from high-performance liquid chromatography (HPLC) can be found in Figure S2). Figure 2c respectively plots the profiles of the amount of MB released from NPs and those that remained in NPs as a function of time (i.e., evolution of the MB absorption peak intensity from both supernant and NPs within the testing period). A decrease of MB absorption in the NPs occurred simultaneously with an increase of that in the supernatant, suggesting the release of MB from NP to the solution. An interesting feature observed in the absorption

dx.doi.org/10.1021/ja3123015 | J. Am. Chem. Soc. 2013, 135, 5709–5716

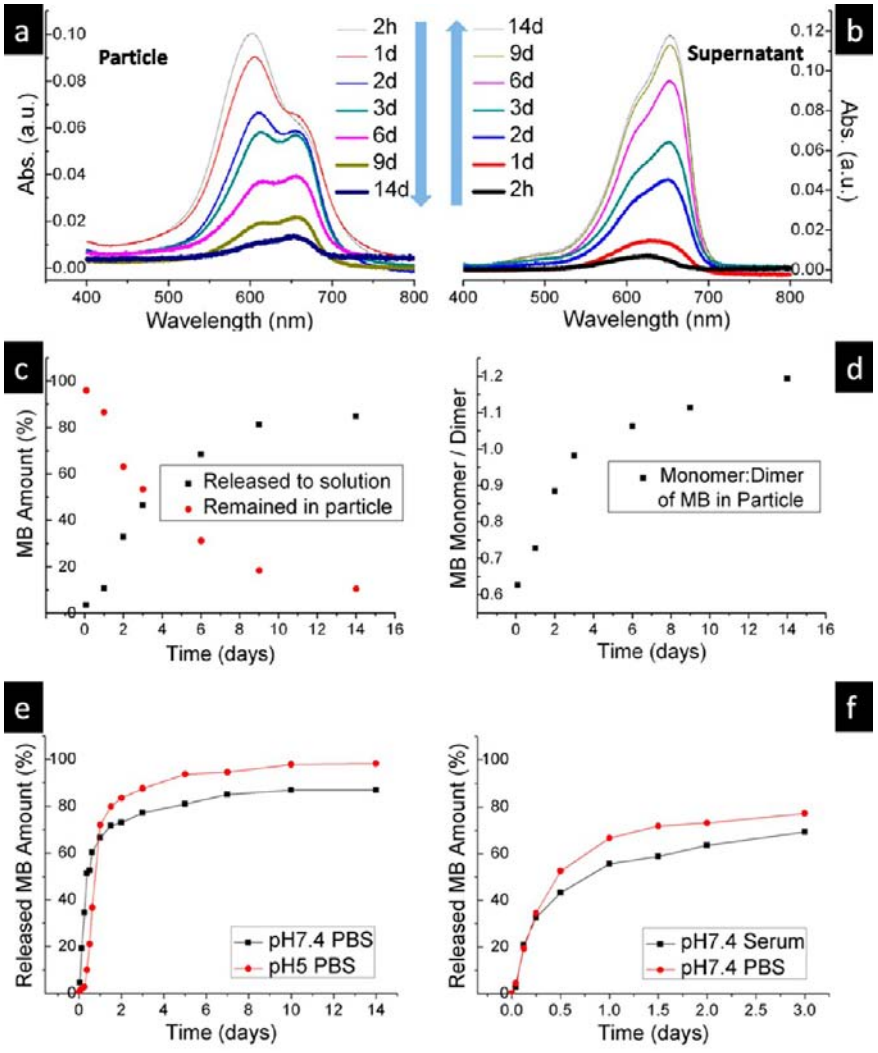

Figure 2. Release of MB from the SiO_2-MB NPs. Absorption spectra of (a) the SiO_2-MB NPs and (b) the supernatant after the NPs have been immersed in deionized water at room temperature for 2 h and 1−3, 6, 9, and 14 days. (c) Evolution of the MB released into supernatant and MB remained in particle as a function of immersing duration (calculated from the absorption maximum peak intensity in a and b). (d) The ratio evolution of the MB monomer/dimer (665/600 nm) in the NPs as a function of immersing duration. Evolution of the MB released from the NPs as a function of the immersing duration (as calculated from the absorption maximum peak intensity of supernatant) investigated (e) in PBS with different pH values, pH 7.4 and pH 5, respectively, and (f) at pH 7.4, in different medium, i.e., serum and PBS at 37 °C.

spectra of the NPs was the intensity variation of the monomer and the dimer absorption peaks, the ratio evolution of the two was plotted in Figure 2d. With less and less MB being left in the NPs, the monomer absorption started to take the lead, while the dimer absorption dominated at the beginning for the as-synthesized NP. In fact, the dominance switching from dimer to monomer can be controlled to occur at different time points, by adjusting the initial MB and tetraethyl orthosilicate (TEOS) amount during NP growth (Figure S3).

In order to simulate in vivo situations, we have also carried out two sets of experiments. In the first one, we compared the drug release in phosphate buffered saline (PBS) at 37 °C at two different pH values, i.e., pH ∼ 7.4 (normal physiological conditions) and ∼5 (intracellular conditions of cancer cells), respectively. Our results showed that the drug release from the NPs was faster at pH ∼ 7.4 in the first 24 h but became slower than that at pH ∼ 5 afterward (Figure 2e). In the second set of experiments, the pH was controlled ∼7.4, and PBS or serum was used as medium for the inspection of drug release from the NPs. A lower drug release rate was obtained in serum than in PBS (Figure 2f), likely due to the protein coating absorbed on the surface of NPs when using serum as the medium.

The corresponding morphological evolution of the SiO_2-MB NPs (sample M1) was recorded using TEM (Figure 3a−d). Most of the NPs remained intact at day 1, while obvious hollow feature appeared in the center of many of the NPs after 4 days immersion. Such center-hollow features continued to enlarge in the following days, leaving a spherical shell of SiO_2 with thinner and thinner shell thickness. At day 9, some of the nanoshells appeared as partially damaged (marked by arrows in Figure 3c), and even longer duration (after 10 days) led to complete collapse of the nanoshell structure to scattered fragments (Figure 3d), coinciding with the MB releasing pattern suggested by the time-dependent absorption spectra (Figure 2). In fact, >95% of the Si (from fragmented SiO_2 NPs) was found in the supernant after their 14 days immersion in deionized water (Figure 3e). The decomposition profile (as measured by the Si amount in the supernatant) of the SiO_2-MB NPs was also examined at pH 7.4 in PBS at 37 °C (Figure 3f) and in simulated body fluid at 37 °C (Figure 3g). The NP

dx.doi.org/10.1021/ja3123015 | J. Am. Chem. Soc. 2013, 135, 5709−5716

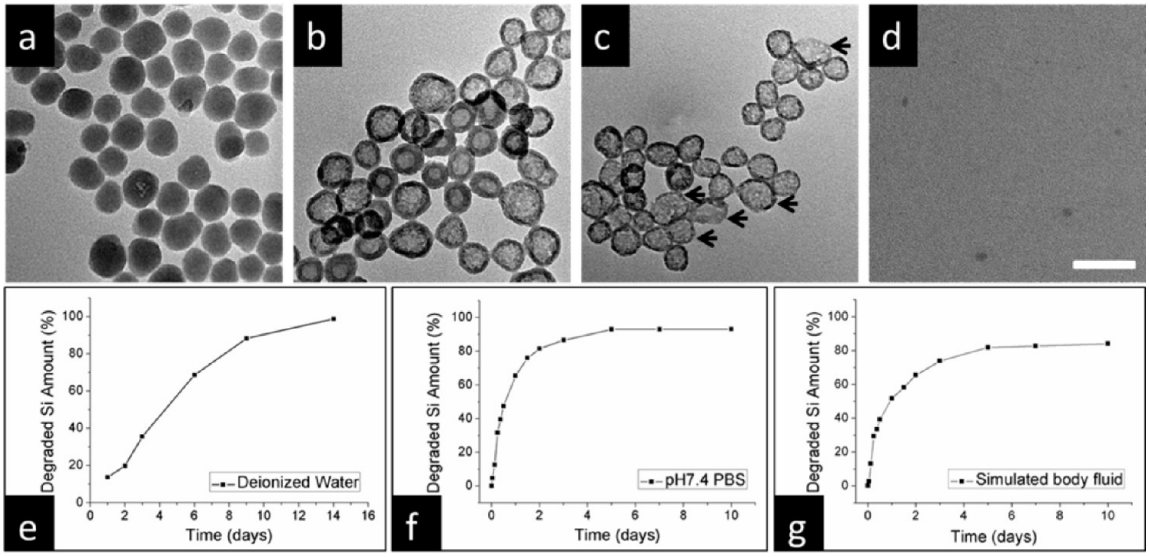

Figure 3. Carrier decomposition of SiO_2-MB NPs. Typical TEM images of the SiO_2-MB NPs after being immersed in deionized water for (a) 1, (b) 4, (c) 9, and (d) 14 days, respectively. The scale bar is 100 nm. ICP-OES result of degraded silicon amount as a function of immersion duration in (e) deionized water at room temperature, (f) PBS (pH 7.4), and (g) simulated body fluid (with 50% FBS) at 37 °C.

decomposition was found to occur the fastest in PBS and the slowest in deionized water.

Release of MB from the SiO_2 NP carrier was also inspected in vitro. After being incubated with the SiO_2-MB NPs for acertain period of time, cell samples were examined by both confocal microscopy and TEM. Celluar uptake of the NPs was confirmed by the MB fluorescence signal in the cells (Figure 4a), after their being incubated with the NPs for 24 h.The NPs were known to enter the cell interior via endocytosis,[26] a direct consequence of which was the NPs' residing in membrane bounded vesicles as aggregates (Figure S4). As a result, the concentrated MB fluorescence signal observed in a randomly spotted pattern in the cells (Figure 4a,b) suggested that most of the MB molecules were confined inside the NPs at the end of 24 h incubation. Similar results (Figure S6a,b) were obtained when using dense SiO_2 NPs containing MB, in which MB is known to be stably confined within the dense SiO_2 NP carrier. (Basic characterizations of the dense SiO_2-MB NPs can be found in the Figure S5). Although both types of NPs (self-decomposable vs dense) were amorphous in nature, porosimetry measurement showed that the self-decomposable NPs were characterized by larger surface area (45.404 m^2/g) and pore volume (0.3239 mL/g), in comparison with those of the dense NPs (surface area 16.787 m^2/g and pore volume 0.0787 mL/g). A 48 h incubation of cells, respectively, with the two types of NPs (the dense one and self-decomposible one) disclosed an intriguing difference between the two cell samples. The spotted fluorescence pattern remained in dense SiO_2-MB NP treated cells, and a stronger intensity was observed (Figure S6c,d), due to continuous uptake of NPs by the cell during the prolonged incubation period. As a comparison, most of the concentrated fluorescence spots in the self-decomposable SiO_2-MB NP treated cells faded, while a rather diffusive fluorenscence background was observed, with intense fluorescence spots only occasionally found (Figure 4c,d). A reasonable explanation to the experimental observation was that MB escaped from the NPs and was eventually released to cytoplasma. The release of MB in vitro was also measured quantitatively. We had incubated the cells with both self-decomposable and dense SiO_2-MB NPs for two different durations (i.e., 24 and 48 h) and compared the amount of MB released to the cytoplasma per cell. A striking difference between the cells treated with the self-decomposable and dense SiO_2-MB NPs can be observed, i.e, the amount of MB released from the self-decomposable NPs was an order of magnitude higher than that of the dense ones (Figure 4e). Further support of the MB release pattern came from TEM, as one can find that NPs remain in the endo/lysosome, but become porous/shell-like as MB escaped (Figure S7).

The MB release/SiO_2 decomposition rate can be manipulated by controlling the source MB concentration during the NP growth. Figure 5 compared the morphology evolution of three SiO_2-MB NP samples (M1−M3 with MB loading amount as 75, 110, and 230 μg MB/mg NP, respectively.) After being dispersed in deionized water for 2 days, the morphology of sample M1 was hardly changed with only small hollow features emerging from the center of the NPs. When the initial MB concentration was higher (sample M2), distinct nanoshell structures were observed after 2 days. Further increase in the initial MB concentration (sample M3) resulted in slightly different morphology for the as-synthesized NPs, i.e., the aggregated MB molecules in the center of the NPs gave brighter contrast in the TEM image (Figure 5e) due to its lower mass thickness as compared to that of SiO_2. At the end of two days, complete rupture of many NPs was observed, in addition to the hollow nanoshells with very thin shell thickness.

Drug Release and Carrier Decomposition Mechanism. The above experimental results suggested possible control over the drug release with simultaneously carrier decomposition, which was driven by a diffusion controlled mechanism. The radial MB concentration gradient from inner out served as a major driving force for MB release. The center-out-first releasing pattern was primarily determined by the growth characteristic of MB molecules within the SiO_2 NPs. At the beginning of the synthesis, very small amount of silica species presented, as they were not directly added as source chemicals but produced from the TEOS hydrolysis. As a comparison, MB was directly added as the source molecules, so its concentration

dx.doi.org/10.1021/ja3123015 | J. Am. Chem. Soc. 2013, 135, 5709−5716

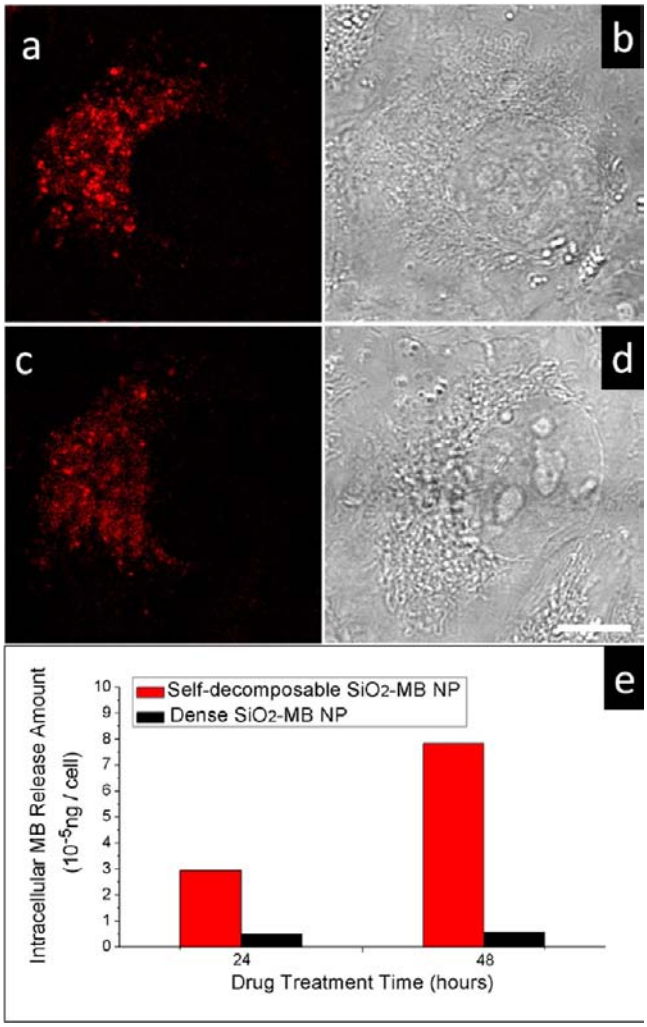

Figure 4. Observation of MB release in vitro. Confocal microscopy images of the H1299 cells treated with self-decomposable SiO_2-MB NPs for (a) 24 and (c) 48 h. Fluorescence signal (red color) from MB with corresponding transmittance images (b) and (d) showing the morphologies of the specific cells. The scale bar is 10 μm. (e) The amount of MB molecules released into cytoplasma after incubating the cells with self-decomposable or dense SiO_2-MB NPs for 24 and 48 h, respectively.

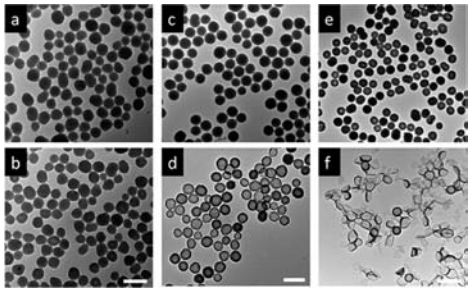

Figure 5. Controllable drug release and self-decomposition of SiO_2-MB NPs. TEM images of the freshly prepared SiO_2-MB NPs (top row) and those after being imersed in deionized water for 2 days (bottom row). Samples (a,b) M1, (c,d) M2, and (e,f) M3. The scale bar is 100 nm for (a,b), 200 nm for (c,d), and 2 μm for (e,f).

was the highest at the start of the synthesis. In the presence of small amount of silica species, MB molecules were then driven to aggregate (Figure S8) due to the opposite charge of MB and silica species (the later serving as "glue" for MB molecule aggregation).[27] These aggregated MB molecules (entangled with very small amount of silica species) became the "nuclei" for further growth of SiO_2-MB NP. As the TEOS hydrolysis persisted and NP growth process proceeded, more and more silica species were produced, while the MB source was continuously consumed as the NP got larger. With such a pattern, high MB concentration occurred in the center of the NPs, agreeing well with the experimentally observed spatial distribution of the compositional elements. A key factor for the formation of "MB-rich nuclei" was the maintenances of high MB concentration and low silica species (from TEOS hydrolysis) concentration at the beginning of the growth. Experimentally, one can either choose to use high MB initial concentration (ranging from 85 to 850 μM in the present case) or limit the silica species initial concentration (by controlling the TEOS hydrolysis rate) to form the "MB-rich nuclei" and obtain the self-decomposable NPs. The latter can be done by adjusting the ammonia amount, which was controlled at <1.08% vol in the present case. When such conditions were not satisfied, one obtained dense NPs, which was commonly reported in the literature.[16]

To support the diffusion controlled mechanism, we carried out another control experiment, i.e., by dispersing the SiO_2-MB NPs into benzene, in which MB was not soluble, neither the MB release nor the SiO_2 NP decomposition occurred (Figure S9). In fact, the SiO_2-MB NP was very stable after being dried; neither MB escaped nor SiO_2 decomposition occurred after months when they were stored in the powder form.

Chemical reaction between the SiO_2 and the MB can be completely ruled out (Figure S10) as a possible reason for SiO_2 carrier decomposition. Such decomposition was triggered by the out-escaping of MB molecules. The decomposition started from the center of the NPs, as suggested by the time-dependent morphological change of the NPs, when they were dispersed in MB soluble solvent (Figure 3). This was reasonable as the center of the NP was mainly composed of high-concentration MB with little SiO_2 incorporated, so that the carrier "bone" structure was the most vulnerable in the center. As MB molecules continuously moved out of the NPs, the SiO_2 "network" (as they grow together with the MB during NP formation) was damaged, eventually leading to complete collapse of the NPs when all drug molecules were released. Consequently, the higher MB concentration in the source material during NP growth, the faster the release of the MB and decay of the SiO_2 carrier (Figure 5). Eventually the carriers completely dissolved into small enough species, which content is biologically benign. The urine of rats were collected at different time points after injection of SiO_2-MB NPs (sample M4), and the Si amounts were detected by ICP-OES (Figure 6a). This in vivo result showed a significant amount of Si excretion via urine using the self-decomposable SiO_2-MB NPs, as compared to that using dense SiO_2-MB NPs. Consistent results were obtained in the biodistribution study of the NPs. Similar to many other nanomaterials,[28−30] the injected SiO_2-MB NPs accumulated mainly in the mononuclear phagocytic system-related organs, such as the liver and the spleen (Figure 6b). However, the self-decomposable SiO_2-MB NPs had a significantly lower accumulation amounts in the corresponding organs compared to those of dense SiO_2-MB NPs at 48 h after injection. This was attributed to their easy degradation followed by fast excretion via the renal system.

dx.doi.org/10.1021/ja3123015 | J. Am. Chem. Soc. 2013, 135, 5709−5716

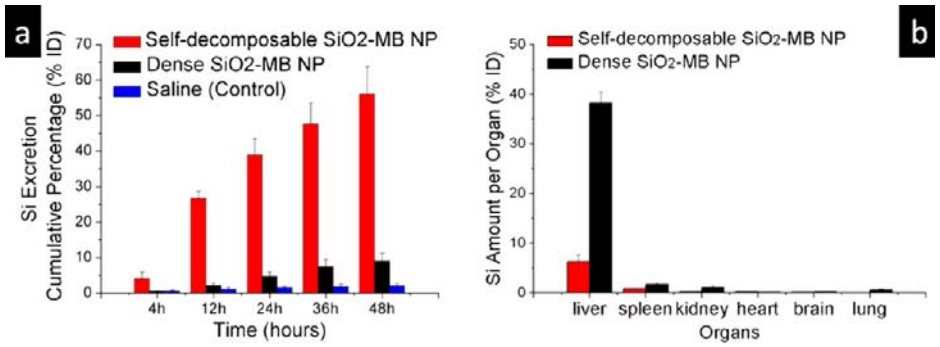

Figure 6. Urinary excretion and biodistribution of SiO_2-MB NPs. (a) ICP-OES analysis of Si amount in the urine of rats collected at 4 12, 24, 36, and 48 h after injection of self-decomposable, dense SiO_2-MB NPs or saline (as the control). (b) ICP-OES analysis of Si amounts in the organs of rats collected at 48 h after injection of self-decomposable and dense SiO_2-MB NPs. The percentages are calculated by the average amount of Si detected compared to the total injection amount of SiO_2-MB NPs. Data are presented with mean ± SEM, n = 3.

Such self-decomposing mechanism can be applied to many different SiO_2-carrier NP systems. Here we gave a few additional examples. Different dye molecules (such as oxazine725 and LDS751) had been incorporated into the SiO_2 NPs, and similar dye release and carrier decomposition had been observed (Figure S11). In addition, we had also incorporated a different drug molecule, i.e., doxorubicin (Dox), into the SiO_2 NPs. Figure 7a shows the optical absorption of such NPs. The characteristic absorption peak of Dox at ∼490 nm can be observed from the NPs dispersed in aqueous solution, suggesting successful loading of the drug into the NPs. The release profile of Dox from the NPs (pH 7.4 PBS at 37 °C) is shown in Figure 7b. The cumulative release of Dox could reach ∼75% within 7 days at the present loading concentration (72 μg Dox/mg NP).

Release of Dox from the self-decomposable NPs was also visualized using confocal microscopy. After being incubated with such NPs for a certain period of time (24 and 48 h), the intracellular distribution of the NPs and the Dox release was examined using a Dox fluorescence signal in the range of 550 nm∼625 nm (excited by using 476 nm laser). Concentrated Dox fluorescence signal was observed in a randomly spotted pattern in the cells, suggesting that most Dox molecules were confined inside the NPs (which were in the endo/lysosomes) at the end of 24 h incubation (Figure 7c,d). After another 24 h (i.e., the 48 h time point), most of the concentrated fluorescence spots faded, while a rather diffusive fluorescence background was observed, (Figure 7e,f) indicating that the Dox molecules escaped from the NPs and were eventually released to cytoplasma. This pattern was similar to that of the MB release. The amounts of Dox released in the cells were also determined quantitatively (Figure 7g).

On the other hand, the corresponding decomposition of such NPs was illustrated by the morphological evolution of NPs using TEM images taken as a function of time (Figure 8). One can observe that the hollow feature starts from the center of the NP, eventually leading to complete fragmentation of the NP, being identical to that of the SiO_2-MB NPs.

CONCLUSION

In conclusion, controlled release and carrier decomposition can be simultaneously realized using a special type of SiO_2 carrier-drug composite NPs. A structural feature of the NP carrier-drug is that the drug molecules are highly concentrated in the NP center and that a loose SiO_2 network is entangled with the drug molecule in the NP. Drug release is primarily determined by diffusion and further triggers the SiO_2 carrier decomposition. This unique feature would enable the NP carrier drug avoid renal filtration at first, leading to prolonged drug residence time in the bloodstream. After complete release of the drug, the carrier structure can be decomposed to small fragments for easy system excretion. The model system of SiO_2-MB NPs is a simplest case in growth due to the opposite charge between MB and the silica species. To incorporate neutral and/or negatively charged molecules, one can either modify the interaction between the silica species and the desired chemical molecules[31,32,15] or employ an absorbing mechanism[4] for loading the neutral and/or negatively charged molecules into an existing self-decomposable NP system. In this way, the present methodology can be generally applied to a wide range of chemical molecules and opens a new direction for nanodrug design.

EXPERIMENTAL SECTION

Synthesis and Characterization of SiO_2-MB NPs. The SiO_2-MB NPs were synthesized using a conventional method[16] with modified parameters. In a typical procedure, a certain amount of MB (2.5 mg for samples M1 and M4, 5 mg for sample M2, and 25 mg for sample M3) was first added to a mixture of 75 mL ethanol with 3.4 mL 25% (for M1−M3) or 10% (for M4) ammonia−water solution, and after that 0.08 mL TEOS was added. The SiO_2-MB NPs were obtained after stirring for 24 h and washing several times before their being dried. Doxorubicin, oxazine725, and LDS751 were incorporated into self-decomposable NP using similar strategies. The dense SiO_2-MB NPs were synthesized using a published method;[16] briefly, 2.5 mg of MB was added to a mixture of 50 mL ethanol with 5 mL 25% ammonia−water solution, and after that 0.2 mL TEOS was added. The ammonia amount is 2.27% vol, which is more than double of that in synthesizing self-decomposable NPs (<1.08% vol). Such a recipe was known to generate dense SiO_2-MB NP, in which the MB can be stably trapped in SiO_2.[16]

The general morphology and the size distribution of the NPs were characterized using TEM (PhilipsCM120). The EELS was performed in TEM (Tecnai G2, FEG) attached with a Gatan imaging filtering system. The chemical maps of the compositional elements were obtained at the silicon L edge (at 99 eV) and nitrogen K edge (at 401 eV). All of the UV−vis absorption spectra were acquired using HitachiU-3501 UV−vis NIR spectrophotometer.

Characterizations of the Drug Release and Carrier Decomposition Process. The MB release was first examined by dispersing the SiO_2-MB NPs (sample M1, 1 mg/mL) in 10 mL deionized water, PBS, or serum (fetal bovine serum, 50% in pH 7.4 PBS). A series of aliquots (1 mL) of solution was removed at different time points and filtered with a centrifugal filter (molecular weight cut off: 30 000 Da, Millipore) to separate the NPs and supernatant. The NPs were dried

dx.doi.org/10.1021/ja3123015 | J. Am. Chem. Soc. 2013, 135, 5709−5716

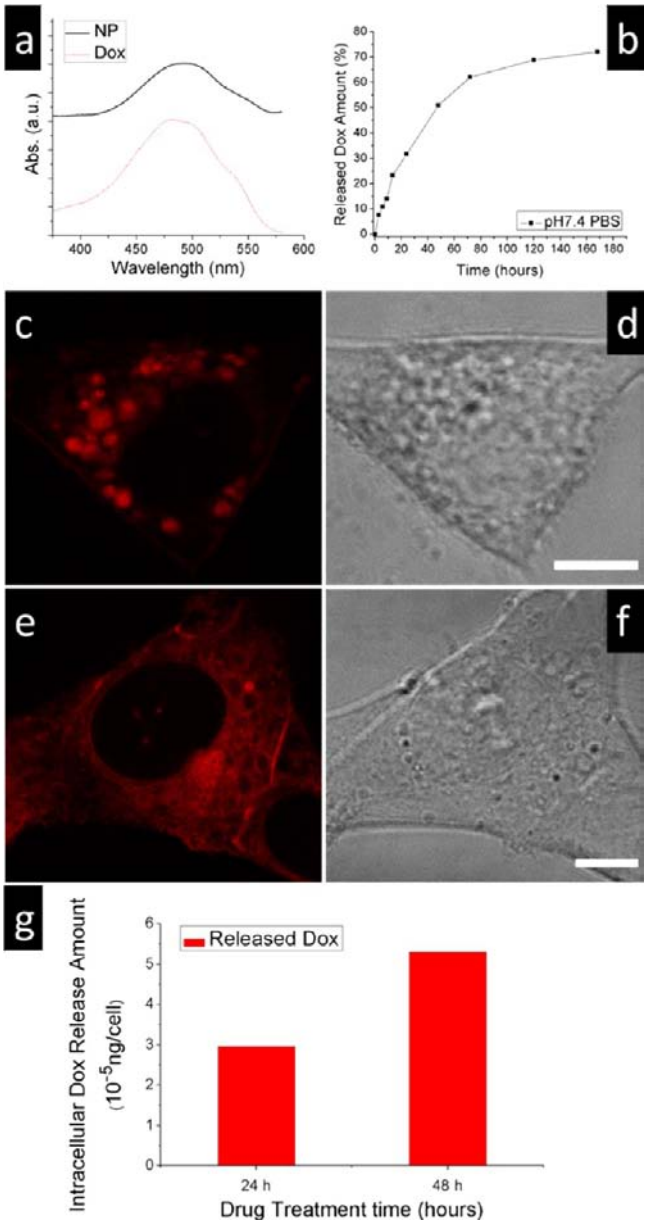

Figure 7. (a) Absorption spectrum (black solid line) showing the successful incorporation of Dox in the NPs. The red dashed line gives the characteristic absorption of pure Dox in aqueous solutions. (b) Evolution of the Dox released from the NPs as a function of immersing duration (calculated from the absorption maximum peak intensity of supernatant) investigated in pH 7.4 PBS at 37 °C. Confocal microscopy images of the cells treated with the NPs for (c) 24 and (e) 48 h. Fluorescence signal (red color) from Dox with corresponding transmittance images (d) and (f) showing the morphologies of the specific cells. The scale bar is 7.5 μm. (g) Amount of Dox released to cytoplasma after incubating the cells with NPs for 24 and 48 h.

and redispersed in deionized water. UV−vis absorption spectra were taken from both redispersed particles solution and supernatants using a Hitachi U-3501 UV−vis NIR spectrophotometer. The degradation of the SiO_2 carrier was monitored by both morphology investigation using TEM and analysis of the above supernatant using inductively coupled plasma optical emission spectrometer (ICP-OES, PerkinEimer Optima 4300 DV).

In vitro experiments were conducted using H1299, human lung carcinoma cells, which were cultured in RPMI 1640 medium, supplemented 10% heat-inactivated fetal bovine serum, 1% streptomycin, and 1% penicillin. The cells were maintained in a standard cell culture incubator at 37 °C in a humidified atmosphere with 5% CO_2. All of the NPs were sterilized by steaming at 115 °C (NPs in powder form) for 2 h and dispersed in the medium by ultrasonication for at least 20 min right before their introduction to the cells. Cells were seeded at initial densities of 5×10^4 cells/mL in flasks (for TEM samples) or dishes (for confocal samples) and incubated for 24 h before introducing NPs (sample M1), and after that the original NP-free medium was discarded, and the fresh prepared NP-containing medium was added. Different cell "feeding time" was adopted, as specified in individual experimental results.

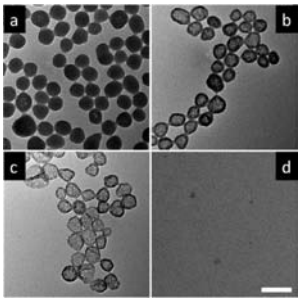

Figure 8. Morphological change of the Dox incorporated NPs. TEM images taken after the NPs' being immersed in deionized water for (a) 1, (b) 4, (c) 9, and (d) 14 days, respectively. The scale bar is 100 nm.

Live NP-fed cells were used for confocal laser scanning microscopy (TCSP5, Leica) with a 63× water-immersion objective lens at 633 nm excitation and 650−700 nm emission. For all TEM studies, the NP-fed cells were fixed with typical procedures that can be found elsewhere.[17] Microtome (Leica, EM UC6) was then used to cut the cured cell cube (in Spurr resin, Electron microscopy sciences, USA) into thin slices (70−90 nm in thickness). The samples were collected on 300-mesh copper TEM grids for observation.

For the quantitative intracellular MB release experiment, the cells were incubated with NPs for a certain period and then washed by PBS several times and counted. After that, the cells underwent lysis by freeze−thaw cycle and were centrifugated ($16000 \times g$) to separate the released MB molecules (into the cytoplasm) from the residual NPs (mainly existing as NP aggregates in the endo/lysosomes). The supernatants containing the released MB molecules were collected, and their optical absorptions were taken to quantify the concentration of the released MB molecules. The average amount of the released MB per cell was calculated by dividing the total MB amount by the cell number.

Urinary Excretion and Biodistribution of SiO_2-MB NPs. For urinary excretion investigation, Sprague−Dawley rats were randomly divided into two groups ($n = 3$) and injected with self-decomposable SiO_2-MB NPs, dense SiO_2-MB NPs (sample M4, 40 mg/kg), or saline (control) through the jugular vein cannula. The special single-rat metabolic cages were used. The urine was collected into separate collection tubes at different time points (4, 12, 24, 36, and 48 h) after injection. The urine samples were then analyzed by ICP-OES for silicon amount. For biodistribution studies, the rats were killed 48 h after injection, and the brain, heart, lung, liver, spleen, and kidney were collected. The tissues were digested and then analyzed for silicon content using ICP-OES.

■ ASSOCIATED CONTENT

Ⓢ Supporting Information

Figures, mainly including TEM image showing intracellular localization of NPs, characteristics of dense SiO_2-MB NPs, confocal images indicating evoluton of the dense SiO_2-MB NPs in cells, TEM observation of carrier decomposition of SiO_2-MB NPs in cells, data of MB release and carrier decomposition in different solvents, test of the chemical reactivity between SiO_2 and MB, and data for extension of the synthetic methodology

dx.doi.org/10.1021/ja3123015 | J. Am. Chem. Soc. 2013, 135, 5709−5716

to other systems. This information is available free of charge via the Internet at http://pubs.acs.org.

AUTHOR INFORMATION

Corresponding Author

liquan@phy.cuhk.edu.hk; linge@cuhk.edu.hk

Notes

The authors declare no competing financial interest.

ACKNOWLEDGMENTS

The work was supported by a direct grant (Project No. 2060438) and UGC equipment grant (SEG_CUHK06).

REFERENCES

(1) Torchilin, V. P. *Nat. Rev. Drug Discovery* **2005**, *4*, 145.
(2) Lee, J. H.; Huh, Y. M.; Jun, Y.; Seo, J.; Jang, J.; Song, H. T.; Kim, S.; Cho, E. J.; Yoon, H. G.; Suh, J. S.; Cheon, J. *Nat. Med. (N. Y., NY, U. S.)* **2007**, *13*, 95.
(3) Oo, M. K. K.; Yang, X.; Du, H.; Wang, H. *Nanomedicine* **2008**, *3*, 777.
(4) Qian, H. S.; Guo, H. C.; Ho, P. C. L.; Mahendran, R.; Zhang, Y. *Small* **2009**, *5*, 2285.
(5) Couleaud, P.; Morosini, V.; Frochot, C.; Richeter, S.; Raehm, L.; Durand, J. O. *Nanoscale* **2010**, *2*, 1083.
(6) Hah, H. J.; Kim, G.; Lee, Y. E. K.; Orringer, D. A.; Sagher, O.; Philbert, M. A.; Kopelman, R. *Macromol. Biosci.* **2011**, *11*, 90.
(7) Vallet-Regi, M. *Chem.−Eur. J.* **2006**, *12*, 5934.
(8) Choi, H. S.; Liu, W.; Misra, P.; Tanaka, E.; Zimmer, J. P.; Ipe, B. I.; Bawendi, M. G.; Frangioni, J. V. *Nat. Biotechnol.* **2007**, *25*, 1165.
(9) Poland, C. A.; Duffin, R.; Kinloch, I.; Maynard, A.; Wallace, W. A. H.; Seaton, A.; Stone, V.; Brown, S.; MacNee, W.; Donaldson, K. *Nat. Nanotechnol.* **2008**, *3*, 423.
(10) Derfus, A. M.; Chan, W. C. W.; Bhatia, S. N. *Nano Lett.* **2004**, *4*, 11.
(11) Park, J. H.; Gu, L.; von Maltzahn, G.; Ruoslahti, E.; Bhatia, S. N.; Sailor, M. J. *Nat. Mater.* **2009**, *8*, 331.
(12) Popplewell, J. F.; King, S. J.; Day, J. P.; Ackrill, P.; Fifield, L. K.; Cresswell, R. G.; Di Tada, M. L.; Liu, K. *J. Inorg. Biochem.* **1998**, *69*, 177.
(13) Lin, W. S.; Huang, Y. W.; Zhou, X. D.; Ma, Y. F. *Toxicol. Appl. Pharmacol.* **2006**, *217*, 252.
(14) Wottrich, R.; Diabate, S.; Krug, H. F. *Int. J. Hyg. Environ. Health* **2004**, *207*, 353.
(15) Tang, L.; Fan, T. M.; Borst, L. B.; Cheng, J. J. *ACS Nano* **2012**, *6*, 3954.
(16) Tada, D. B.; Vono, L. L. R.; Duarte, E. L.; Itri, R.; Kiyohara, P. K.; Baptista, M. S.; Rossi, L. M. *Langmuir* **2007**, *23*, 8194.
(17) Giri, S.; Trewyn, B. G.; Stellmaker, M. P.; Lin, V. S. Y. *Angew. Chem., Int. Ed.* **2005**, *44*, 5038.
(18) Rosenholm, J. M.; Peuhu, E.; Eriksson, J. E.; Sahlgren, C.; Linden, M. *Nano Lett.* **2009**, *9*, 3308.
(19) Tu, H. L.; Lin, Y. S.; Lin, H. Y.; Hung, Y.; Lo, L. W.; Chen, Y. F.; Mou, C. Y. *Adv. Mater.* **2009**, *21*, 172.
(20) Trewyn, B. G.; Whitman, C. M.; Lin, V. S. Y. *Nano Lett.* **2004**, *4*, 2139.
(21) Agostini, A.; Mondragón, L.; Bernardos, A.; Martínez-Máñez, R.; Marcos, M. D.; Sancenón, F.; Soto, J.; Costero, A.; Manguan-García, C.; Perona, R.; Moreno-Torres, M.; Aparicio-Sanchis, R.; Murguía, J. R. *Angew. Chem., Int. Ed.* **2012**, *51*, 10556.
(22) Coll, C.; Mondragón, L.; Martínez-Máñez, R.; Sancenón, F.; Marcos, M. D.; Soto, J.; Amorós, P.; Pérez-Payá, E. *Angew. Chem., Int. Ed.* **2011**, *50*, 2138.
(23) Li, Z.; Barnes, J. C.; Bosoy, A.; Stoddart, J. F.; Zink, J. I. *Chem. Soc. Rev.* **2012**, *41*, 2590.
(24) Yang, P.; Gai, S.; Lin, J. *Chem. Soc. Rev.* **2012**, *41*, 3679.
(25) Vivero-Escoto, J. L.; Slowing, I. I.; Wu, C.-W.; Lin, V. S. Y. *J. Am. Chem. Soc.* **2009**, *131*, 3462.
(26) Chu, Z. Q.; Huang, Y. J.; Tao, Q.; Li, Q. *Nanoscale* **2011**, *3*, 3291.
(27) Severino, D.; Junqueira, H. C.; Gugliotti, M.; Gabrielli, D. S.; Baptista, M. S. *Photochem. Photobiol.* **2003**, *77*, 459.
(28) Lee, J. H.; Huh, Y. M.; Jun, Y.; Seo, J.; Jang, J.; Song, H. T.; Kim, S.; Cho, E. J.; Yoon, H. G.; Suh, J. S.; Cheon, J. *Nat. Med.* **2007**, *13*, 95.
(29) Liu, Z.; Davis, C.; Cai, W. B.; He, L.; Chen, X. Y.; Dai, H. J. *Proc. Natl. Acad. Sci. U.S.A.* **2008**, *105*, 1410.
(30) Choi, H. S.; Liu, W.; Misra, P.; Tanaka, E.; Zimmer, J. P.; Ipe, B. I.; Bawendi, M. G.; Frangioni, J. V. *Nat. Biotechnol.* **2007**, *25*, 1165.
(31) Lee, C.-H.; Cheng, S.-H.; Wang, Y.-J.; Chen, Y.-C.; Chen, N.-T.; Souris, J.; Chen, C.-T.; Mou, C.-Y.; Yang, C.-S.; Lo, L.-W. *Adv. Funct. Mater.* **2009**, *19*, 215.
(32) Rossi, L. M.; Silva, P. R.; Vono, L. L. R.; Fernandes, A. U.; Tada, D. B.; Baptista, M. c. S. *Langmuir* **2008**, *24*, 12534.